Generation of Zonal Map From Point Data via Weighted Skeletonization by Influence Zone

H. M. Rajashekara, Pratap Vardhan, and B. S. Daya Sagar, *Senior Member, IEEE*

***Abstract*—Data about many variables are available as numerical values at specific geographical locations. We develop a methodology based on mathematical morphology to convert point-specific data into zonal map. This methodology relies on weighted skeletonization by zone of influence that determines the points of contact of multiple frontlines propagating, from various points spread over the space, at the traveling rates depending upon the variable's strength. We demonstrate this approach for converting rainfall data available at specific rain gauge locations (points) into a spatially distributed zonal map that suggests zones of equal rainfall.**

***Index Terms*—Dilation, dilation-propagation speed, marker, mask, mathematical morphology, points, skeletonization by influence zone (SKIZ), zones.**

I. Introduction

REMOTELY sensed satellite data act as source to prepare domain-specific thematic maps by applying digital image processing techniques (e.g., filtering, segmentation, classification, etc.). However, there exist several important variables for which only location-specific data are available. Numerous data available over a geographical space are in point form. Such point-specific data facilitate visualization in statistical form. Visualization of such point-specific data in geographical form evidently requires a procedure to convert point-specific data into zonal form. Such conversion approach by using computer-assisted techniques and spatial statistical tools has significance in the following: 1) integrating thematic information retrieved from multiscale multitemporal remotely sensed satellite data with other variables for which only location-specific data are available; 2) spatiotemporal modeling of various phenomena and processes; and 3) visualizing relationships between the geographic variables in terms of spatial form.

Manuscript received June 14, 2011; revised August 8, 2011; accepted September 15, 2011. Date of publication November 3, 2011; date of current version March 7, 2012. The work of B. S. D. Sagar was supported by the Indian Statistical Institute under Internal Grant SSIU-01.

This paper has supplementary downloadable material available at http://ieeexplore.ieee.org, provided by the authors. This includes one multimedia AVI format movie clip, which shows animation of rainfall zone map generated by using the proposed approach. This material is 9.76 MB in size.

H. M. Rajashekara is with the Central Computer Centre, Bangalore Centre, Indian Statistical Institute, Bangalore 560059, India (e-mail: raja@isibang.ac.in).

P. Vardhan is with the Department of Electronics and Communication Engineering, Maulana Azad National Institute of Technology, Bhopal 462051, India (e-mail: pratapapvr@gmail.com).

B. S. D. Sagar is with the Systems Science and Informatics Unit, Bangalore Centre, Indian Statistical Institute, Bangalore 560059, India (e-mail: bsdsagar@isibang.ac.in).

Color versions of one or more of the figures in this paper are available online at http://ieeexplore.ieee.org.

Digital Object Identifier 10.1109/LGRS.2011.2169489

A conventional approach to convert such point data into polygonal form is Thiessen polygon construction where the space is divided into polygons with the rain gauge in the middle of each polygon assumed to be representative for the rainfall on the area of land included in its polygon. These polygons are made by drawing lines between gauges and then making perpendicular bisectors of those lines form the polygons. In Geographical Information Science (GISci), this method was adapted to analyze space use [1], [2]. The zone (area) of an influence map could be generated via Thiessen polygon method which resembles a convex polygon. There exists traditional and geostatistical interpolation method [3] such as simple kriging.

This letter presents an algorithm using mathematical morphology [4], particularly weighted-skeletonization-by-influence-zone (WSKIZ) transformation, to convert point-specific data, and also variable-specific data, into zonal map. Several researchers have employed mathematical morphology in the contexts of GISci [5]–[9], geosciences [10]–[12], and remote sensing [13]–[25]. This WSKIZ approach—an alternative to Voronoi diagrams that are used in geophysics and meteorology to analyze spatially distributed data (such as rainfall measurements)—can be used to describe the area of influence of a point in a set of points possessing varied values (rainfall values, etc.).

The organization of this letter is as follows. In Section II, binary morphological dilation and its multiscale representations are introduced. Model and algorithm concepts, motivation, and methodology to convert point-specific value data into zonal map form are explained in Section III. Section IV provides the results drawn in terms of zonal map for a variable (e.g., rainfall) available as numerical values at specific points over the geographical space out of demonstrations and the respective discussion of the significance of the obtained results. Section V provides the concluding remarks.

II. Morphological Dilation

Morphological dilation of a set (A), on the 2-D Euclidean discrete space Z^2, is one of the important morphological operators [4]. Structuring element (B)—that possesses characteristic information such as shape, size, orientation, and origin—acts as a probing rule to perform this operation on set A. We consider a B that is symmetric with respect to the origin, circle in shape (on eight connectivity grids), and of primitive size of 3×3. The morphological dilation of A by symmetric B $(A \oplus B)$ that expands A by B

$$A \oplus B = \{a : (B)_a \cap A \neq \emptyset\} = \bigcup_{b \in B} A_b \tag{1}$$

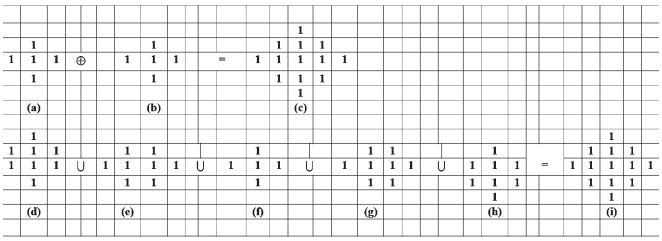

Fig. 1. (a) Set A with five foreground elements shown with 1s. (b) Structuring element B of size 3×3 and symmetric about the origin at center. (c) Dilation of A by B. (d)–(h) Five translates of each element of A by B for dilation. (i) Dilation of A by B obtained by taking the union of five translates shown in (d)–(h).

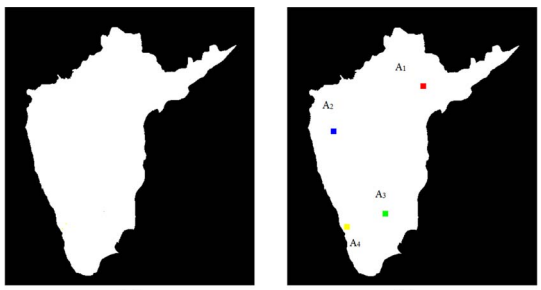

Fig. 2. (a) Region considered is South India and (b) gauge-station locations (A_1, A_2, A_3, and A_4).

where A_b denotes the *translation* of A along the vector b, $A_b = \{a + b | a \in A\}$, and $\hat{B} = \{a : -a \in B\}$ is the *symmetric* of B with respect to the origin. An illustrative example explaining morphological dilation is shown in Fig. 1.

In the proposed approach, the characteristic information of B plays a vital role. Multiscale dilation can be generated by increasing the size of structuring element nB, where $n = 0, 1, 2, \ldots, N$. Iterative dilations by primitive size B for n times $(A \oplus nB)$ are needed as

$$(A \oplus nB) = ((A \oplus B) \oplus B \oplus \cdots \oplus B). \tag{2}$$

III. Conversion of Point-Specific Values Into Zonal Map via WSKIZ

A. Location-Specific Data Over Geographical Space

Let S be the underlying space, endowed with a distance d, and A [mask, Fig. 2(a)] be a subset of S consisting of several locations as points [e.g., Fig. 2(b)] where the time-varying data such as rainfall and temperature values are available. Fig. 2(b) shows four points (gauge stations), and each point (A_i) possesses a value that denotes strength of a variable. Such a map with points in a map satisfies the following morphological relationship: $(A_i \cap A_j) = \emptyset$ for $i \neq j$.

B. Model to Generate Zonal Map From Point Data

We propose an algorithm based on mathematical morphology to generate zonal map from point data. This algorithm consists of the following steps.

1) Consider the point-specific values (e.g., rainfall, temperatures, etc.) as points (markers) such that they act as markers from which the propagations compete to fill the geodesic space (i.e., global mask).
2) Sort and rank the points according to the corresponding strengths of a geographic variable (e.g., rainfall values).
3) Such ranking allows assigning to each marker a specific rate at which it competes to fill the available space. When there are several markers assigned with different strengths of a variable, the rates at which those markers need to be expanded will decide the final sizes and shapes of the influence zones in the zonal map constructed.

Treating each point as a lake (marker), by simulating flood propagation process, the water frontlines generated from corresponding lakes that are spatially distributed over a Cartesian space would extinguish (meet) each other at various places. By preserving all such extinguishing points, while suppressing all other details, we obtain *SKIZs*. This process can be simulated with ease as there are no constraints imposed on flood propagation speed. In other words, when the propagation speed of flood waters originating from spatially distributed lakes is uniform, it is easy to visualize the SKIZ. However, for the purpose of converting point data into zonal map, the propagation speed of flood frontlines needs to be made point dependent, based on the variable's strength at that point. Treating the original map (A) as the mask [Fig. 2(a)] and the points of a map as multiple markers [e.g., Fig. 2(b)], recursive geodesic dilations (3) with marker-dependent propagation speeds simultaneously from multiple markers would provide a WSKIZ. Such a WSKIZ is the zonal map, where the specified variable strength determines the dilation-propagation speeds. The entire process requires the following steps.

Step 1) Let points A_i denote locations (gauge stations) at which the values of a variable (e.g., rainfall) are available.
Step 2) Compute recursive geodesic dilations of each point A_i by means of primitive structuring element B of size λ_i that is location and value of a variable-dependent.
Step 3) Compute WSKIZ by systematically performing recursive geodesic dilations with location-dependent propagation speeds simultaneously from multiple points to compute all possible extinguishing points [(4) and (5)].
Step 4) Represent each zone with a specific color such that no two neighboring zones have similar colors.

In the sections that follow, we provide details of the aforementioned sequential steps involved in converting point data into zonal map.

Computation of Point-Dependent Recursive Geodesic Dilations: Dilation-propagation speed is assigned to points according to the variable strength. The stronger the variable strength, the faster the dilation-propagation speed of the point per unit time step [e.g., Fig. 4(d)]. For the purpose of performing point-dependent geodesic dilations, each point A_i is assigned to be dilated by a structuring element of primitive size of λ_i, where λ denotes the primitive size of B and i denotes the index of the point. Then, the geodesic dilation of A_i by B of primitive size λ_i takes the form

$$(A_i \oplus nB_{\lambda_i}) \cap A = \delta^{n}_{\lambda_i}(A_i) \tag{3}$$

where nB_{λ_i} denotes structuring element B of primitive size λ_i that depends upon the point-dependent variable strength (propagation speed) for n cycles (n ranging from $1, 2, \ldots, N$). The intersection between mask (A) and the version of A_i dilated by nB_{λ_i} for $n = 1$ time yields the first level of geodesic dilation of A_i, $\delta^n_{\lambda_i}(A_i)$.

Computation of Zonal Map via WSKIZ: Let $Z(A_i)$ be a zone of (A_i). In the process of converting the point data into polygonal map, the two steps involved include

$$Z(A_i) = \bigcup_n \left(\delta^n_{\lambda_i}(A_i) \cap A\right) \setminus \bigcup_{\forall j} \left(\delta^n_{\lambda_{j\neq i}}(A_j) \cap A\right) \quad (4)$$

$$Z(A) = \left(\bigcup_i (Z(A_i))\right)^C \quad (5)$$

where each zone of map $Z(A_i)$ is computed by a three-step approach: 1) subtracting the union of marker (A_j) zones other than (A_i) $(A_{j\neq i})$ geodesically dilated simultaneously by structuring element of point-dependent primitive size from the geodesically dilated version of (A_i) by structuring element of primitive size dependent on (A_i); 2) taking the union of such subtracted versions for all n values ranging from 0 to N to obtain the map zone for the zone of the map (A_i); and 3) taking the complement of the union of all obtained map zones to yield WSKIZ, which is, in other words, the converted point data into zonal map. In (4), A denotes mask [e.g., Fig. 2(a)]. If the regions occupied by mountains are subtracted from the mask (A), then we can generate zonal map only within the nonmountainous regions by employing (4). Such a mask that excludes mountainous regions (geographical hurdles) is essential while employing this approach to simulate flood propagation.

Assignment of Colors to ZA_i: Let ZA_i denote a zone obtained for a point A_i. For example, let us assume that there are four zones obtained for four different points [Fig. 2(b)] and each zone possesses spatially distributed values [Fig. 2(b)]. According to the positions of these zones, different colors will be assigned such that no two neighboring zones will be assigned with similar colors. With such a color-coding scheme, it is easier to identify zones. However, in realistic cases, we may need to assign similar weights to multiple points. Under such circumstance, zones obtained need to be further merged based on the similar weights adopted.

All these steps explained in Sections III-A and B are demonstrated on four points shown in Fig. 2(b) by assigning arbitrarily different propagation speeds.

C. Model Demonstration

A total N number of points A_i (locations) that denote, for instance, in 2-D discrete space, Z^2 [Fig. 2(a)] is considered. Four gauge stations $(A_1, A_2, A_3, \text{and } A_4)$ shown [Fig. 2(b)] are considered to demonstrate the proposed approach. The four possible zones that one can visualize to be within the mask [Fig. 2(a)] by imposing varied propagation speeds of dilation are shown in Fig. 3(a)–(d). We assume that these point data represent some time-varying parameters such as rainfall and temperature for a specified time. If these point data depict four different strengths, then generation of zonal map requires

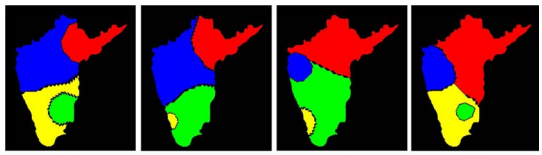

(a) (b) (c) (d)

Fig. 3. Variable strengths (in terms of propagation speeds) are given as (a) $A_2 > A_4 > A_1 > A_3$, (b) $A_2 > A_1 > A_3 > A_4$, (c) $A_1 > A_3 > A_2 > A_4$, and (d) $A_1 > A_4 > A_2 > A_3$.

TABLE I
RANKS ACCORDING TO VARIABLE STRENGTHS FOR THE POINTS. I, II, AND III DENOTE POINT INDEX, RAINFALL VALUES, AND WEIGHTS, RESPECTIVELY. READER CAN FIND MORE DETAILS ABOUT SEQUENTIAL STEPS INVOLVED IN IMPLEMENTATION OF WSKIZ (FIG. S1) AND THE BOUNDARIES OF DILATION PROPAGATIONS FROM THE POINTS TO THE STATE OF REACHING THE CONVERGENCE (FIG. S2, S3) AT http://www.isibang.ac.in/~bsdsagar/GRSL-00335-2011-FIG-S1-S3-Supporting-Material.pdf

I	II	III	I	II	III
A_1	214.5	6	A_{18}	4.4	2
A_2	181.3	5	A_{19}	9.2	2
A_3	31.8	2	A_{20}	11.6	2
A_4	9.2	2	A_{21}	96.6	3
A_5	56.1	3	A_{22}	45.9	2
A_6	35.3	2	A_{23}	58.6	3
A_7	69.2	3	A_{24}	18.9	2
A_8	8.9	2	A_{25}	30.1	2
A_9	6.8	2	A_{26}	0.0	1
A_{10}	1.4	2	A_{27}	168.1	5
A_{11}	8.6	2	A_{28}	92.5	3
A_{12}	129.2	4	A_{29}	100.3	4
A_{13}	0.0	1	A_{30}	34.7	2
A_{14}	119.0	4	A_{31}	52.8	3
A_{15}	252.6	6	A_{32}	33.9	2
A_{16}	36.9	2	A_{33}	1.6	2
A_{17}	179.1	5	A_{34}	3.6	2

point-data-specific propagations to generate zonal map. Four zonal maps, each zone assigned with a color [Fig. 3(a)–(d)], are generated for four different point-specific sequences with the following order: 1) $A_2 > A_4 > A_1 > A_3$; 2) $A_2 > A_1 > A_3 > A_4$; 3) $A_1 > A_3 > A_2 > A_4$; and 4) $A_1 > A_4 > A_2 > A_3$. In the model, we have shown that there are four zones after assigning colors to zones in each panel [Fig. 3(a)–(d)] obtained by four different weighting schemes.

Generated zones shown in Fig. 3 could be better compared with those of polygons constructed based on Thiessen polygon and Voronoi diagram construction approaches. However, the WSKIZ approach has advantages over the other approaches for three reasons: 1) it has straightforward implementation of algorithms; 2) weights could be assigned to generate weight-based zonal maps; and 3) it could be fully automated.

IV. EXPERIMENTAL RESULTS

We consider a map depicting 34 locations [gauge stations; Fig. 4(a)], spread across India, at which rainfall values are recorded for the period of March–April 2011 to demonstrate the applicability of the algorithm explained in Section III. According to the rainfall values (Table I), weights are assigned for dilation-propagation speed for each gauge station. The higher the rainfall recorded, the larger the assigned weight is. The larger the weight, the faster the propagation speed. Table I provides the details of these weights for all the 34 points for the rainfall variable.

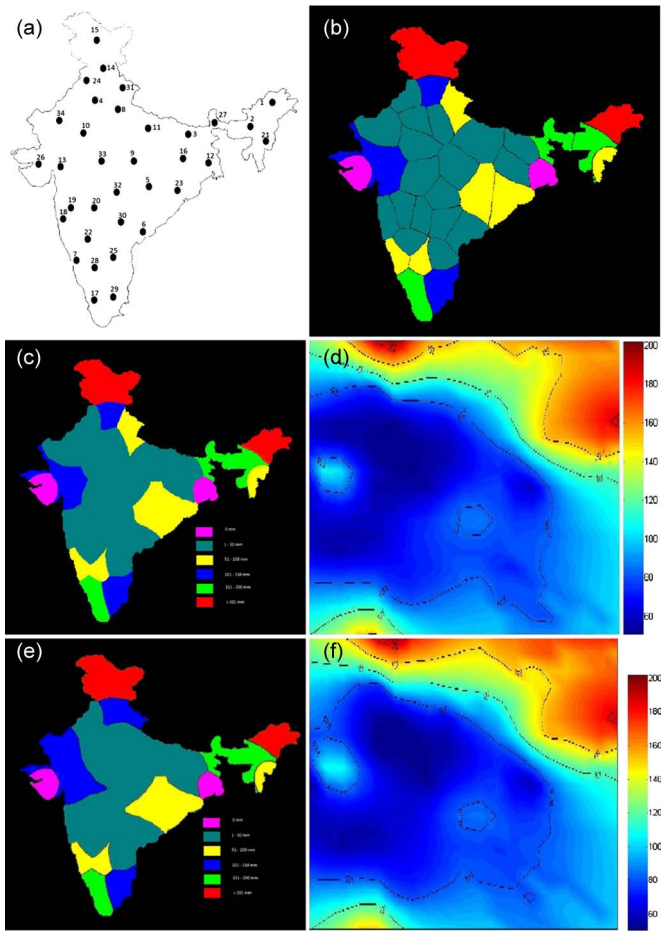

Fig. 4. (a) Thirty-four points (locations) of rain gauge stations spread over India indexed $(A_1 - A_{34})$, (b) rainfall zonal map generated by having various possible propagation speeds, and the variable strengths in terms of propagation speeds are given according to ranks shown in Table I, (c) broader zones obtained after merging the zones [Fig. 4(b)] obtained with similar propagation speeds, (d) kriged map generated for 34 gauge-station data, and (e) and (f) WSKIZ and kriged maps for 29 gauge-station data, where last five stations are dropped from (a). Animation is available at ieeexplore.ieee.org.

By assigning propagation speeds in terms of primitive size of structuring element (λ_i) for respective points of (A_i) and by allowing those points to dilate for n times satisfying the involved processes according to (3)–(5), we converted point data into zonal map [Fig. 4(b)]. This zonal map [Fig. 4(b)] suggests that rainfall at all locations within each zone belongs to a particular station within the zone and, hence, has the same values. Animation of rainfall zone map generated by using the proposed approach is available on ieeexplore.ieee.org. It is seen that the propagation speeds that are rainfall (weight) dependent correspond to boundaries separated by different distances. After zonal map is created by following WSKIZ approach, the zones that could be created with similar propagation speed (weights) are merged [Fig. 4(c)] as six broad zones. The principle involved in merging the zones obtained is that those frontlines propagating at equal speeds (weights) that generate zones are merged and are assigned with similar colors to visualize as a broader zonal map. In this broader zonal map [Fig. 4(c)], if there is n number of weights employed to generate WSKIZ map, there will be n number of colors depicting broader zones [e.g., Fig. 4(c)]. In the zonal maps [Fig. 4(b)], the colors are assigned to each zone to have better demarcation. However, the colors in this figure have no significance. On the other hand, in Fig. 4(c), colors assigned to the broader zones obtained after merging have significance. This broader zonal map [Fig. 4(c)] suggests that rainfall at all locations within each zone belongs to a particular station within the zone and, hence, has the same values. The broad zones from the merged zonal map [Fig. 4(c)] depicted in six colors suggest the following: 1) There are multiple zones [Fig. 4(b)] obtained with similar weights (propagation speeds), and 2) they belong to six different zones depicting six different ranges of rainfall patterns. Kriged map [Fig. 4(d)], generated for the 34 gauge-station data, visually is in good agreement. It is to be noted that, the higher the weight (rainfall) assigned for a specific point, similarly, the higher the propagation speed. We also show WSKIZ map [Fig. 4(e)] and kriged map [Fig. 4(f)] generated by considering first 29 gauge-station data from Fig. 4(a). It is obvious from merged WSKIZ maps [Fig. 4(c) and (e)] generated for 34 and 29 gauge-station data, respectively, that there is significant visual agreement in the spatial distribution of rainfall. For instance, rainfall-wise weights for locations (A_1, A_{15}) are highest, and hence, in those zones, shown in rainfall zonal map [Fig. 4(b)] are the zones of high rainfall. The lowest ranked locations in terms of rainfall include A_{13} and A_{26}, and those zones could be seen in Fig. 4(b).

Intensity of the rainfall at the gauge stations enables a zone, the size of which does not need to be proportional to the intensity. Gauge stations with less rainfall intensity recorded may possess larger zone and vice versa. Size of a zone ZA_i is collectively governed by the following factors: 1) intensity (weight) of rainfall at location (A_i); 2) number of gauge stations (A_j) in the proximity of a station (A_i) under question; and 3) intensities of rainfall at those adjacent gauge stations (A_j).

Zonal maps generated by dividing (multiplying) the weights by two are similar to that of the zonal maps shown as long as the rainfall values at the gauge stations are relatively similar in pattern (phase synchronous). Such zonal maps are invariant under dividing (multiplying) weights. If the rainfall values recorded at rain gauge stations are with different patterns, the zonal maps generated from such point-specific rainfall values will significantly differ. Other elegant approaches that have not hitherto been applied in the context of converting point-specific data, of geoscientific interest, into zonal map include watershed transform [26]–[29] and Euclidean distance transform [30]–[32]. These transforms are treated as generalization of SKIZ to arbitrary metrics. It is interesting as an open problem. To generate spatial maps with zones of various intensities—of several phenomena of climatological, ecological, and geomorphological relevance—the underlying physical principle of this proposed technique would very well work. Such maps generated via WSKIZ for time-dependent phenomena (e.g., rainfall and temperature) yield maps that possess varied form of zones that are also time dependent. Such maps generated for different time periods could be used in spatiotemporal modeling. This WSKIZ could be performed in a geodesic manner within the mask that is without the hurdles such as mountains. However, for certain numerical variables such as population densities, this

approach may not be an appropriate one. However, for location analysis, flood modeling, epidemic spread, and thermograph generation, this approach provides insights. Location-specific numerical variable data of relevance to various terrestrial phenomena and processes available as point data could be mapped into continuous display of the sampling patterns by using this approach. Such continuous maps of a time-varying variable generated via this approach for different time periods provide insights to do the following: 1) understand the spatiotemporal behavior of a phenomenon and 2) establish spatial relationships between the phenomena. The main advantage of this approach over the Thiessen polygonal approach is that each influence zone form and structure does not look like a polygon.

V. Conclusion

We have presented an approach to visualize variables available as point values at fixed geographical locations as zonal map based on geodesic dilation propagation whose speed depends upon the location and variable strength. In the zonal map that we generate via the WSKIZ approach, the outline of each zone would be much smoother as we choose primitive structuring element circle in shape. This way of converting point data into zonal map form is uniform and more stable, and this algorithm could be easily programmed. This approach provides insights to integrate variable-specific zonal maps with thematic information retrieved from remotely sensed data.

Acknowledgment

The authors would like to thank Prof. G. Korvin for the suggestions during the preparation of this letter and three anonymous reviewers and Editor Prof. P. Gamba for their suggestions and comments which strengthened this letter.

References

[1] J. Casaer, M. Hermy, P. Coppin, and R. Verhagen, "Analyzing space use patterns by Thiessen polygon and triangulated irregular network interpolation: A non parametric method for processing telemetric animal fixes," *Int. J. Geogr. Inf. Sci.*, vol. 13, no. 5, pp. 499–511, Jul. 1999.

[2] B. Cao and F. Glover, "Creating balanced and connected clusters to improve service delivery routes in logistics planning," *J. Syst. Sci. Syst. Eng.*, vol. 19, no. 4, pp. 453–480, 2010.

[3] N. A. C. Cressie, *Statistics of Spatial Data*. New York: Wiley, 1991.

[4] J. Serra, *Image Analysis and Mathematical Morphology*. London, U.K.: Academic, 1982.

[5] B. Su, Z. Li, G. Lodwick, and J.-C. Muller, "Algebraic models for the aggregation of area features based upon morphological operators," *Int. J. Geogr. Inf. Sci.*, vol. 11, no. 3, pp. 233–246, 1997.

[6] D. Pullar, "MapScript: A map algebra programming language incorporating neighborhood analysis," *Geoinformatica*, vol. 5, no. 2, pp. 145–163, Jun. 2001.

[7] L. T. Tay, B. S. D. Sagar, and H. T. Chuah, "Analysis of geophysical networks derived from multiscale digital elevation models: A morphological approach," *IEEE Geosci. Remote Sens. Lett.*, vol. 2, no. 4, pp. 399–403, Oct. 2005.

[8] B. S. D. Sagar, "Visualization of spatiotemporal behavior of discrete maps via generation of recursive median elements," *IEEE Trans. Pattern Anal. Mach. Intell.*, vol. 32, no. 2, pp. 378–384, Feb. 2010.

[9] S. Aksoy and R. G. Cinbis, "Image mining using directional spatial constraints," *IEEE Geosci. Remote Sens. Lett.*, vol. 7, no. 1, pp. 33–37, Jan. 2010.

[10] B. S. D. Sagar and L. Chockalingam, "Fractal dimension of non-network space of a catchment basin," *Geophys. Res. Lett.*, vol. 31, no. 12, p. L12 502, 2004.

[11] B. S. D. Sagar and L. T. Tien, "Allometric power-law relationships in a Hortonian fractal DEM," *Geophys. Res. Lett.*, vol. 31, no. 6, p. L06 501, 2004.

[12] L. T. Tay, B. S. D. Sagar, and H. T. Chuah, "Granulometric analysis of basin-wise DEMs: A comparative study," *Int. J. Remote Sens.*, vol. 28, no. 15, pp. 3363–3378, Aug. 2007.

[13] B. S. D. Sagar, G. Gandhi, and B. S. P. Rao, "Applications of mathematical morphology on water body studies," *Int. J. Remote Sens.*, vol. 16, no. 8, pp. 1495–1502, 1995.

[14] B. S. D. Sagar, M. Venu, and B. S. P. Rao, "Distributions of surface water bodies," *Int. J. Remote Sens.*, vol. 16, no. 16, pp. 3059–3067, 1995.

[15] M. Pesaresi and J. A. Benediktsson, "A new approach for the morphological segmentation of high-resolution satellite imagery," *IEEE Trans. Geosci. Remote Sens.*, vol. 39, no. 2, pp. 309–320, Feb. 2001.

[16] B. S. D. Sagar, M. B. R. Murthy, C. B. Rao, and B. Raj, "Morphological approach to extract ridge-valley connectivity networks from digital elevation models (DEMs)," *Int. J. Remote Sens.*, vol. 24, no. 3, pp. 573–581, 2003.

[17] J. A. Benediktsson, M. Pesaresi, and K. Arnason, "Classification and feature extraction for remote sensing images from urban areas based on morphological transformations," *IEEE Trans. Geosci. Remote Sens.*, vol. 41, no. 9, pp. 1940–1949, Sep. 2003.

[18] T. Barata and P. Pina, "A morphological approach for feature space partitioning," *IEEE Geosci. Remote Sens. Lett.*, vol. 3, no. 1, pp. 173–177, Jan. 2006.

[19] H. Taubenbock, M. Habermeyer, A. Roth, and S. Dech, "Automated allocation of highly structured urban areas in homogeneous zones from remote sensing data by Savitzky–Golay filtering and curve sketching," *IEEE Geosci. Remote Sens. Lett.*, vol. 3, no. 4, pp. 532–536, Oct. 2006.

[20] J. Chanussot, J. A. Benediktsson, and M. Fauvel, "Classification of remote sensing images from urban areas using a fuzzy possibilistic model," *IEEE Geosci. Remote Sens. Lett.*, vol. 3, no. 1, pp. 40–44, Jan. 2006.

[21] M. Dalla Mura, J. A. Benediktsson, F. Bovolo, and L. Bruzzone, "An unsupervised technique based on morphological filters for change detection in very high resolution images," *IEEE Geosci. Remote Sens. Lett.*, vol. 5, no. 3, pp. 433–437, Jul. 2008.

[22] X. Huang, L. P. Zhang, and L. Wang, "Evaluation of morphological texture features for mangrove forest mapping and species discrimination using multispectral IKONOS imagery," *IEEE Geosci. Remote Sens. Lett.*, vol. 6, no. 3, pp. 393–397, Jul. 2009.

[23] J. Pan, M. Wang, D. R. Li, and J. L. Li, "A network-based radiometric equalization approach for digital aerial orthoimages," *IEEE Geosci. Remote Sens. Lett.*, vol. 7, no. 2, pp. 401–405, Apr. 2010.

[24] B. S. D. Sagar and J. Serra, "Preface: Spatial information retrieval, analysis, reasoning and modelling," *Int. J. Remote Sens.*, vol. 31, no. 22, pp. 5747–5750, Nov. 2010.

[25] M. Dalla Mura, A. Villa, J. A. Benediktsson, J. Chanussot, and L. Bruzzone, "Classification of hyperspectral images by using extended morphological attribute profiles and independent component analysis," *IEEE Geosci. Remote Sens. Lett.*, vol. 8, no. 3, pp. 542–546, May 2011.

[26] F. Meyer, "Topographic distance and watershed lines," *Signal Process.—Mathematical Morphology and its Applications to Signal Processing*, vol. 38, no. 1, pp. 113–125, Jul. 1994.

[27] L. Najman and M. Schmitt, "Watershed of a continuous function," *Signal Process.*, vol. 38, no. 1, pp. 99–112, Jul. 1994.

[28] L. Vincent and P. Soille, "Watersheds in digital spaces: An efficient algorithm based on immersion simulations," *IEEE Trans. Pattern Anal. Mach. Intell.*, vol. 13, no. 6, pp. 583–598, Jun. 1991.

[29] J. Cousty, G. Bertrand, L. Najman, and M. Couprie, "Watershed cuts: Minimum spanning forests and the drop of water principle," *IEEE Trans. Pattern Anal. Mach. Intell.*, vol. 31, no. 8, pp. 1362–1374, Aug. 2009.

[30] T. Hirata, "A unified linear-time algorithms for computing distance maps," *Inf. Process. Lett.*, vol. 58, no. 3, pp. 129–133, May 1996.

[31] A. Meijster, J. B. T. M. Roerdink, and W. H. Hesselink, "A general algorithm for computing distance transform in linear time," in *Mathematical Morphology and Its Applications to Image and Signal Processing*. Dordrecht, The Netherlands: Kluwer, 2000, pp. 331–340.

[32] T. Saito and J. I. Toriwaki, "New algorithms for Euclidean distance transformation of an n-dimensional digitized picture with applications," *Pattern Recognit.*, vol. 27, no. 11, pp. 1551–1565, Nov. 1994.